RSC Advances

PAPER

View Article Online
View Journal | View Issue

Cite this: *RSC Adv.*, 2017, **7**, 16777

Enhanced anti-stocks luminescence in $LaNbO_4:Ln^{3+}$ (Ln^{3+} = Yb^{3+}, $Er^{3+}/Ho^{3+}/Tm^{3+}$) with abundant color†

Huining Huang,[a] Haifeng Zhou,[b] Juan Zhou,[c] Tao Wang,[a] Dapeng Huang,[a] Yaqiang Wu,[a] Leilei Sun,[a] Guangjun Zhou,*[a] Jie Zhan[a] and Jifan Hu[a]

Received 23rd December 2016
Accepted 1st March 2017

DOI: 10.1039/c6ra28592a

rsc.li/rsc-advances

Lanthanide ion doped up-conversion luminescent (UCL) materials, which have the ability to convert near-infrared longer wavelength excitation light into shorter wavelength visible light, have recently drawn much attention. Now, a series of Ln^{3+} (Yb^{3+}, $Er^{3+}/Ho^{3+}/Tm^{3+}$) ions doped $LaNbO_4$ (LNO) materials were prepared through a two-step route, including a facile sol–gel process and subsequent combustion. In our work, thermogravimetric and differential thermal analysis (TG-DTA), X-ray diffraction (XRD), field emission scanning electron microscopy (FE-SEM), up-conversion luminescence (UCL), energy level diagram, luminescent lifetimes and corresponding CIE were utilized to characterize the properties. A 980 nm laser was employed to excite Yb^{3+} ions to achieve the $^2F_{7/2} \rightarrow {}^2F_{5/2}$ transition, and the LNO:Yb^{3+},$Er^{3+}/Ho^{3+}/Tm^{3+}$ samples exhibited intense green, yellowish-green and blue emission, respectively. Luminescent spectra at different powers demonstrated the two-photon absorption process; meanwhile, the corresponding energy transfer mechanisms from Yb^{3+} to Ln^{3+} and the emissions of Ln^{3+} under 980 nm laser excitation were described *via* an energy level diagram. Moreover, multicolor UCL emissions, the optimal intensities and corresponding mechanism were systematically explored *via* a suite of concentration spectra of different Ln^{3+} ions. At last, the decay lifetimes based on the concentration variation of Yb^{3+} ion demonstrated that the lifetimes are heavily influenced by Yb^{3+} ion.

1. Introduction

Up-conversion luminescence (UCL), a process that can convert near-infrared excitation into visible emission, also known as anti-Stokes shift, has recently gained more and more attention.[1–8] The energy transfer process, in which two or more low-energy photons are converted into one high-energy photon, has great potential applications in laser materials, data storage, near-infrared quantum counters, solar energy, traditional light, display technologies, biological imaging and so on.[9–20] Multiple metastable levels of the lanthanides just perfectly meet the requirement of these applications. The lanthanides are filled with the 4f-shell which range from element lanthanum (La) to lutetium (Lu), and their trivalent ions (Ln^{3+}) generally possess several excited 4f energy level except for La^{3+}, Yb^{3+}, Ce^{3+}, and Lu^{3+}. Because the unique 4f–4f transitions of Ln^{3+} are shielded by the $5s^2$ and $5p^6$ sub-shells, weak electron–phonon are coupling and consequently sharp and narrow f–f transition bands are come into being. Besides, the f–f transitions are Laporte forbidden which can lead to low transition probabilities and substantially long-lived excited states.[21] Therefore, rare-earth doped up-conversion materials are extremely available for varied application.

UCL can be achieved by singly doped and double doped materials. Ln^{3+} ions such as Er^{3+}, Ho^{3+} and Tm^{3+}, which have abundant ladder-like arranged energy levels, are usually employed as activators in the UCL materials. However, the capacity absorbing cross-sections of Ln^{3+} is extremely low, and in turn the UCL intensity of singly doped materials is overall low. Additionally, high doping levels can result in harmful cross-relaxation and quenching excitation energy. Therefore, it is essential to reduce the concentration of Ln^{3+} and avoid the quenching effect. As a consequence, a sensitizer which has an abundant absorption cross-section in the near-infrared range is usually co-doped to enhance the UCL intensity. Trivalent Yb possesses an extremely simple energy level structure, including only one ground state level and one excited state level. In addition, the excited state level of Yb^{3+} is higher than the metastable energy levels of the representative up-converting Ln^{3+} (Er^{3+}, Ho^{3+}, and Tm^{3+}) and the $^2F_{7/2} \rightarrow {}^2F_{5/2}$ transition is perfectly resonant with them because the energy state pair of Ln^{3+} is closed to the energy gap of Yb^{3+} (10^4 cm^{-1}). With the

[a]State Key Laboratory of Crystal Materials, Shenzhen Research Institute, Shandong University, Jinan 250100, P. R. China. E-mail: gjzhou@sdu.edu.cn
[b]School of Materials Science and Engineering, Qilu University of Technology, Jinan 250353, P. R. China
[c]Center for Disease Prevention and Control of Jinan Military Command, Jinan 250014, P. R. China

† Electronic supplementary information (ESI) available. See DOI: 10.1039/c6ra28592a

assistance of Yb^{3+}, a relatively low (less than 0.02) content of the up-converting activators can realize the UCL emission. In the experiments, the optimal concentrations of Er^{3+}/Ho^{3+}/Tm^{3+} are 0.02, 0.005 and 0.003, respectively. In our work, the Yb^{3+} ions with excellent optical characteristics are employed as a sensitizer in high-efficiency UCL materials.

Beyond that, it is extremely vital to find a suitable host compound with outstanding optical properties. Firstly, ideal host materials should be inorganic compounds with trivalent rare-earth ions, which ascribe to the similar ionic size and chemical properties of the whole rare-earth ions. Secondly, ideal host materials also require low lattice phonon energy, which can reduce non-radiative loss to increase the radiative emission. Although heavy halides and fluorides exhibit low phonon energy (less than 300 cm^{-1} and 350 cm^{-1}), the applications are still limited due to their hygroscopic and instability. In comparison, oxides exhibit higher thermal and chemical stability, so appropriate oxides with relatively low phonon energy have more promising application. The third influencing factor is the crystal structure, which can be imputed to the difference of the crystal-fields around activators in various symmetrical matrices. Compared with high symmetry hosts, low symmetry hosts have more probability to achieve f–f transition for up-converting Ln^{3+}, and this is because the electronic coupling between 4f energy levels and electronic configuration. Furthermore, the reduction of cation size in the host can lead to the enhancement of the crystal-field around the doped ions and subsequently increase UCL intensity.

Up to now, a series of niobates such as $YNbO_4$, $LaNbO_4$, $GdNbO_4$, $CaNb_2O_6$ have showed good mechanical and chemical stability, thus they have attracted widespread attention. Lin group have demonstrated that the niobates are a commendable host material in the down-conversion emission.[22–24] La^{3+} possesses the biggest radius which can be replaced by the other rare-earth ions and the symmetry of $LaNbO_4$ is pretty low, which are beneficial to enhance the optical properties, thus we select $LaNbO_4$ as our host material.

As far as we know, as of now, the UCL properties of niobate have rarely been reported. In our work, LNO and Ln^{3+} doped LNO have been fabricated *via* a facile sol–gel and combustion method. In general, the adulteration of various rare-earth ions is the easiest way to achieve multicolor in the UCL emission. Under the irradiation of 980 nm laser, four-color emissions from UCL materials $NaYbF_4$:Tm/Ho/Er/Yb were first demonstrated by Nann *et al.*[25] In our work, an array of up-conversion luminescent properties, including the up-conversion mechanism, power-dependent spectra, concentration-dependent spectra, lifetimes and CIE chromaticity coordinates. Additionally, we find the optimal concentration to achieve the strongest UCL intensities. It indicates that the samples have great prospect for applications such as 3D display and solid-state lasers.

2. Experimental

2.1. Synthetic procedures

A sequence of nano/micro-materials with chemical composition of $La_{1-(y+e/h/t)}NbO_4$:yYb^{3+},eEr^{3+}/hHo^{3+}/tTm^{3+} (y = 0.02–0.25, e = 0.005–0.04, h = 0.0025–0.02, t = 0.001–0.006), where La atoms occupations were considered to be occupied by other rare earth atoms, were synthesized by a facile sol–gel combustion process. Stoichiometric amounts of high-purity chemical compounds, including lanthanum oxide (La_2O_3), ytterbium oxide (Yb_2O_3), erbium oxide (Er_2O_3), holmium oxide (Ho_2O_3), thulium oxide (Tm_2O_3), niobium oxide (Nb_2O_5), citric acid ($C_6H_8O_7 \cdot H_2O$) and ammonium nitrate (NH_4NO_3), were used as the raw materials. The synthetic method is a two-step route, involving the sol–gel progress and the high-temperature combustion progress. First, $La(NO_3)_3$, $Yb(NO_3)_3$, $Ho(NO_3)_3$ and $Er(NO_3)_3$ aqueous solutions were prepared by dissolving the calculated amount of La_2O_3, Yb_2O_3, Er_2O_3, Ho_2O_3 and Tm_2O_3 into diluted nitric acid at a certain mole ratio, respectively. The residual nitric acid was removed *via* heating and evaporation. Second, excess hydrofluoric acid (HF, 40%) was employed to dissolve niobium oxide (Nb_2O_5, 99.9%) at 90 °C and the pH was regulated to 9.0 by adding aqueous ammonia solution, then a white precipitate of $Nb_2O_5 \cdot nH_2O$ was obtained. Subsequently, the precipitate was washed with deionized water repeatedly by centrifugation to guarantee that the F^- ion was entirely removed. Third, citric acid and ammonium nitrate were used to dissolve the precipitate with a mole ratio of 3 : 5 : 1. In this process, citric acid and ammonium nitrate play the roles of complexant and fuel, respectively. Fourth, the RE nitrates were dissolved in the above solution under continuous stirring at a constant temperature of 85 °C to form the homogeneous sol. The transparent sol became a white gel with high viscosity by evaporating the water. After drying the gel for 12 h at 110 °C, a nut-brown precursor was formed. The precursor was directly annealed in air for 3 h at 1000 °C in a furnace and cooled down to room temperature naturally to obtain the final product.

2.2. Characterization

Thermal analysis of the precursor was performed on a thermogravimetric-differential thermal analyser (TG-DTA) (Perkin Elmer Corporation, Diamond TG-DTA) from 30 °C to 1100 °C with a constant heating rate of 20 °C min^{-1}. The X-ray diffraction (XRD) measurements were carried out on a Germany Bruker Axs D8-Focus diffractometer with graphite-monochromatized Cu Kα radiation (λ = 0.15418 nm) at a scanning rate of 0.04 s per step over the 2θ range from 10° to 80°. The morphology and size of the products were obtained using a scanning electron microscope (SEM, Hitachi, S-4800). The UCL spectra, decay times and were recorded on fluorescence spectrometer (Edinburgh FLS 980) equipped with a tuneable 980 nm semiconductor (1 W laser) as the excitation source.

3. Results and discussion

3.1. Structural, phase and morphological analysis

The TG-DTA curves of pure LNO precursor xerogel powder dried for 12 h at 110 °C is shown in Fig. 1. Throughout the temperature range from 30 °C to 1100 °C, there are three main weight loss stages in the TG curve. The first stage is from room temperature to 235 °C. In this stage, the evaporation of water,

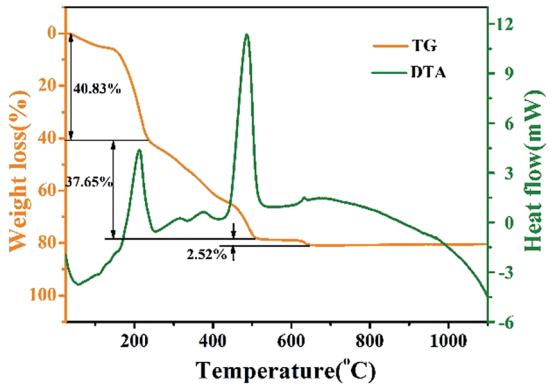

Fig. 1 TG-DTA curves of pure LNO precursor xerogel powder.

the combustion of organic phases (such as citric acid) and the thermal decomposition of NO_3^- collectively result in weight loss (at approximately 40.83%), an endothermic peak (at approximately 57 °C) and a strong exothermic peak (at approximately 212 °C). At the second stage, throughout which the temperature ranges from 235 °C to 508 °C, the weight loss is about 37.65%, and a high-intensitive exothermic peak occurs at 486 °C, which can be ascribed to the further combustion of the remaining organic materials. The last stage of weight loss occurring between 508 °C and 645 °C is about 2.52%, corresponding to a faint exothermic weak at 632 °C, which is mainly because of the process of the phase transformation from tetragonal to monoclinic and higher crystallization. The tetragonal phase can not be existent under high temperature.[26] No obvious weight loss is observed above 632 °C, which indicates that all organic compounds in the precursor had been decomposed completely below 632 °C, and the crystallized LNO inorganic phase is formed.

The composition, crystal structure, and phase purity of the as-prepared samples LNO host under various temperatures and times, LNO:0.10Yb^{3+},0.02Er^{3+}, LNO:0.15Yb^{3+},0.005Ho^{3+} and LNO:0.15Yb^{3+},0.003Tm^{3+} are respectively determined from the XRD patterns, which are clearly shown in Fig. 2. All of the diffraction peaks could be well matched with the XRD pattern of monoclinic $LaNO_4$ phase corresponding to standard reference JCPDS card no. 81-1973. As shown in Fig. 3, the crystallization belongs to monoclinic system, and space group is $I112/b$ (15), and cell parameters are $a = 5.5634$ Å, $b = 5.2030$ Å, $c = 11.5227$ Å, $V = 332.69(3)$ Å^3, and $Z = 4$. Significantly, as the annealing temperature increases from 500 °C to 1000 °C and reaction time grows from 0.5 h to 3 h, the diffraction peaks become obviously stronger and sharper, implying that the high annealing temperature and longer reaction time contribute to the high crystallinity of the samples. Based on the higher crystallinity of the heat treated samples, we can choose more appropriate condition to prepare the samples. In general, the samples along with high crystallinity show higher emission intensity. Further, no traces of impurity phases are observed, demonstrating little change of this crystal structure accompanied by introducing such Yb^{3+}, Er^{3+}, Ho^{3+} and Tm^{3+} ions into the host. This is because such Ln^{3+} ions have similar radius and the La^{3+} ions is

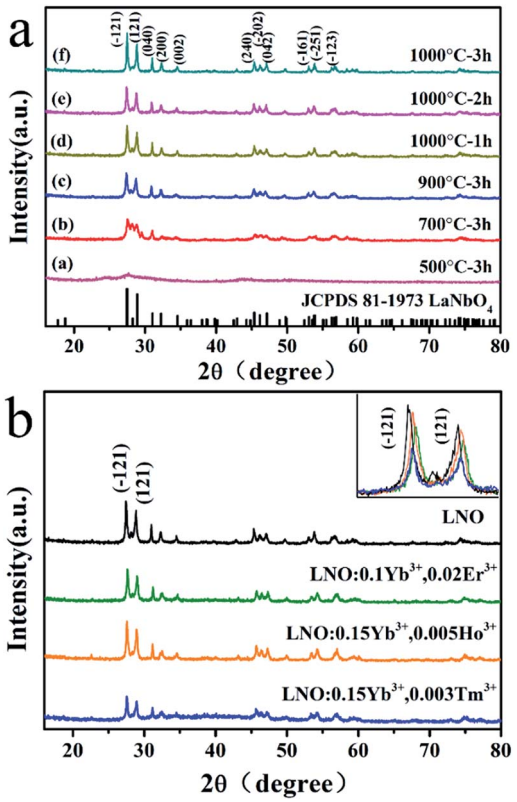

Fig. 2 XRD patterns of the as-prepared (a) $LaNbO_4$ host with different temperature, time and the standard pattern (JCPDS 81-1973) of $LaNbO_4$. (b) $LaNbO_4$:0.10Yb^{3+},0.02Er^{3+}, LNO:0.15Yb^{3+},0.005Ho^{3+}, LNO:0.15Yb^{3+},0.003Tm^{3+} samples.

just located at the central position surrounded by eight oxygen atoms and the $LaNbO_4$ phase has a low symmetry crystal structure. Only one kind of La cationic position with a Wyckoff position 4e could be taken in for activators due to the analogical ionic radius of La^{3+} [$r = 1.061$ Å, CN = 8], Yb^{3+} ($r = 0.858$ Å, CN = 8), Er^{3+} ($r = 0.881$ Å, CN = 8), Ho^{3+} ($r = 0.894$ Å, CN = 8) and Tm^{3+} ($r = 0.87$ Å, CN = 8). Furthermore, in the inset of Fig. 2, the diffraction peaks (−121) (121) are slightly shifted to a higher degree and the crystallinity lower down accompanied with Yb^{3+}, Er^{3+}/Ho^{3+}/Tm^{3+} doped into the host material.

The SEM images of the as-prepared LNO, LNO:0.10-Yb^{3+},0.02Er^{3+}, LNO:0.15Yb^{3+},0.005Ho^{3+}, LNO:0.15Yb^{3+},0.003Tm^{3+} samples are shown in Fig. 4. It can be clearly found that the

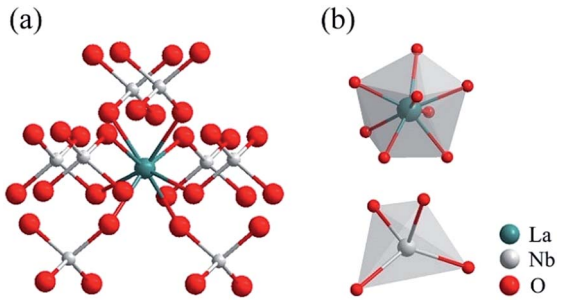

Fig. 3 Crystal structure of the monoclinic $LaNbO_4$ phase.

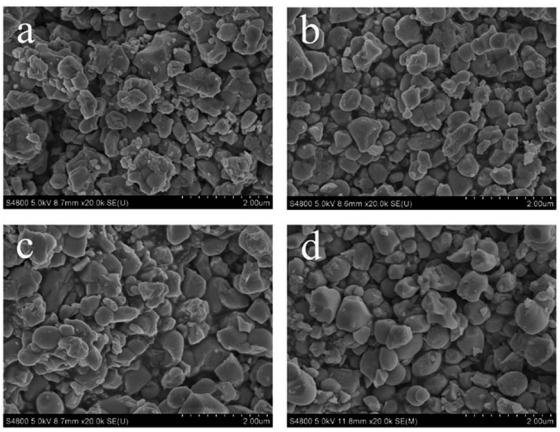

Fig. 4 SEM images of the as-prepared (a) LNO, (b) LNO:0.10-Yb^{3+},0.02Er^{3+}, (c) LNO:0.15Yb^{3+},0.005Ho^{3+}, (d) LNO:0.15Yb^{3+},0.003Tm^{3+}.

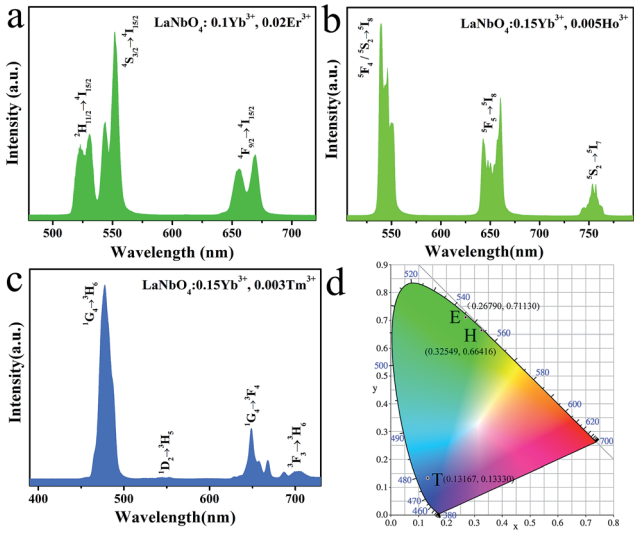

Fig. 5 The up-conversion emission spectra of (a) LNO:0.10-Yb^{3+},0.02Er^{3+}, (b) LNO:0.15Yb^{3+},0.005Ho^{3+}, (c) LNO:0.15Yb^{3+},0.003Tm^{3+}, (d) the CIE chromaticity coordinates of the as-prepared samples under the 980 laser excitation.

morphology and particle size of the as-prepared samples have been slightly influenced by the dopant, which is corresponding to the XRD patterns.

The agglomeration of the samples is observed especially in undoped LNO sample, which is attributed to the high-temperature combustion process. The morphology and size of the samples are not comparatively homogeneous based on the same reason. The diameter of all the samples ranges from 200 nm to 500 nm except that the morphology become more uniform along with Yb^{3+}, Er^{3+}, Ho^{3+}, Tm^{3+} co-doped in LNO. The TEM images which shown in Fig. S1† are also demonstrated the phenomenon.

3.2. Upconversion photoluminescence properties and mechanism

In order to obtain multicolor in the UCL, Er^{3+}, Ho^{3+}, Tm^{3+} together with Yb^{3+} are doped in LNO, respectively. The UCL spectra of LNO:Yb^{3+},Er^{3+}/Ho^{3+}/Tm^{3+} under 980 nm excitation and their corresponding CIE (Commission Internationale de l'Eclairage 1931 chromaticity) coordinates positions are shown in Fig. 5. Sharp characteristic emission peaks are all obvious in the UCL spectra. Fig. 5a exhibit the UCL spectrum of the as-prepared LNO:0.10 Yb^{3+},0.02 Er^{3+} and there are mainly two typical emission bands. The shorter-wavelength (green) emission in the range of 510 to 580 nm, corresponding to the transition from the excited state $^2H_{11/2}$ and $^4S_{3/2}$ to the ground state $^4I_{15/2}$. While the longer-wavelength (red) emission ranging from 635 to 690 nm, which belongs to $^4F_{9/2} \rightarrow {}^4I_{15/2}$ transition of Er^{3+}. Because the intensity of the green emission is obviously stronger than the red emission, the final color is green and CIE chromaticity diagram for it is (0.26790, 0.71130) as shown in Fig. 5d(E) under the excitation of 980 nm laser.

Fig. 5b shows the UCL spectrum of the as-prepared LNO:0.15Yb^{3+},0.005Ho^{3+}, radiative relaxation processes of $^5F_4/^5S_2 \rightarrow {}^5I_8$, $^5F_5 \rightarrow {}^5I_8$ and $^5S_2 \rightarrow {}^5I_7$ levels corresponding to green (about 540 nm), red (about 660 nm) and NIR (about 753 nm) emissions, respectively. In addition, the CIE chromaticity coordinates of LNO:0.15Yb^{3+},0.003Ho^{3+} is (0.32549, 0.66416) shown in Fig. 5d(H) under the excitation of 980 nm laser.

Fig. 5c displays the UCL spectrum of the as-prepared LNO:0.15Yb^{3+},0.003Tm^{3+}, which exhibit one extremely strong blue emission, one weak green emission and two very weak red emission ascribed to $^1G_4 \rightarrow {}^3H_6$ (located at 475 nm), $^1D_2 \rightarrow {}^3H_5$ (between 515 nm to 560 nm) and $^1G_4 \rightarrow {}^3F_4$, $^3F_3 \rightarrow {}^3H_6$ (ranging from 625 nm to 720 nm) respectively. The final color is relative pure blue and CIE chromaticity diagram is (0.13167, 0.13330) as shown in Fig. 5d(T) under the excitation of 980 nm laser.

As is well-known to all, the UCL is an anti-Stokes luminescent process, in which two or more low-energy photons are consecutively absorbed and followed by emission of a higher-energy photon in quick succession.[27] To explore the populating mechanism, the up-conversion luminescent properties are compared at different powers, which are shown in Fig. 6a–c. According to the spectra, the transition intensity of the as-prepared samples becomes stronger corresponding to the increasing pump powers.

For any unsaturated UCL process, the visible emission intensity (I_{em}) and the pump power P of infrared excitation resource is expressed as

$$I_{em} \propto P^n$$

where n is the positive integer of NIR photons absorbed to convert a higher-energy, which can be required from the slope in Fig. 6d–f.[28–30] By fitting the data points, the slopes of log(I_{em}) *versus* log(P) for the $^2H_{11/2} \rightarrow {}^4I_{15/2}$, $^4S_{3/2} \rightarrow {}^4I_{15/2}$, $^4F_{9/2} \rightarrow {}^4I_{15/2}$ transitions of LNO:0.10Yb^{3+},0.02Er^{3+} are calculated to be 1.865, 1.861 and 1.969, respectively. (shown in Fig. 6d.) The strait lines illustrate that two photons are absorbed in the UCL process. For LNO:0.15Yb^{3+},0.005Ho^{3+}, the slopes at $^5F_4/^5S_2 \rightarrow {}^5I_8$, $^5F_5 \rightarrow {}^5I_8$ and $^5S_2 \rightarrow {}^5I_7$ transitions are 2.041, 2.016 and 2.195, respectively, indicating a two-photon absorption process. (shown in Fig. 6e.) The value of n for LNO:0.15Yb^{3+}/0.003Tm^{3+} are 2.331,

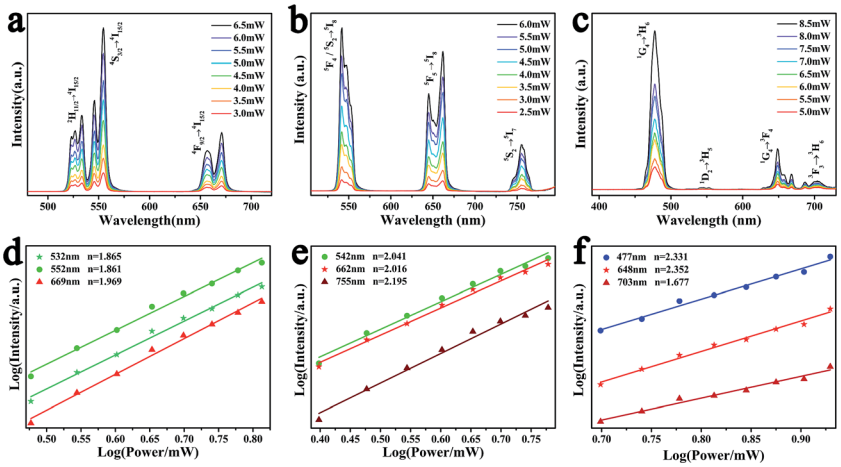

Fig. 6 UCL spectra of the as-prepared (a) LNO:0.10Yb^{3+},0.02Er^{3+}, (b) LNO:0.15Yb^{3+},0.005Ho^{3+}, (c) LNO:0.15Yb^{3+},0.003Tm^{3+} under the excitation of 980 nm laser at the different power and the corresponding power dependence of UCL in (d) LNO:0.10Yb^{3+},0.02Er^{3+}, (e) LNO:0.15Yb^{3+},0.005Ho^{3+}, (f) LNO:0.15Yb^{3+},0.003Tm^{3+}.

2.352 and 1.677, which are corresponding to $^1G_4 \rightarrow {}^3H_6$, $^1G_4 \rightarrow {}^3F_4$ and $^3F_3 \rightarrow {}^3H_6$, respectively, which demonstrate the transition from Yb^{3+} to Tm^{3+} involving two NIR photons. (shown in Fig. 6f.) However, as the photons enter the crystals, the loss of energy and nonluminous relaxation cause the emitted energy to be less than the absorbed energy, and thus the slope is less than 2. But the slopes of Ho^{3+} and Tm^{3+} are nearly more than 2 and this phenomenon illustrates existence of multiphoton absorption in LNO:Yb^{3+},Ho^{3+} and LNO:Yb^{3+},Tm^{3+} samples.

In general, three luminescence mechanism have been proved in the UCL process, and they are ground/excited state absorption (GSA/ESA), energy transfer up-conversion (ETU) and photon avalanche (PA).[31] In the Fig. 6d–f, each slope of all the samples is not changed, which demonstrates PA mechanism is not involved in the UCL process. To explore the UCL populating mechanism, the typical energy level diagrams and the possible mechanism for LNO:Yb^{3+}/Er^{3+}, LNO:Yb^{3+}/Ho^{3+}, LNO:Yb^{3+}/Tm^{3+} are exhibited in Fig. 7a–c. The solid, dotted and curly arrows represent the emission, energy transfer, and multi-phonon relaxation process, respectively. In the Yb^{3+} and Ln^{3+} co-doped LNO samples, Yb^{3+} ions absorb energy from the 980 nm laser excitation, while Er^{3+}, Ho^{3+} and Tm^{3+} generate visible emission. First of all, the ground state $^2F_{7/2}$ of two Yb^{3+} are promoted to the $^2F_{5/2}$ by absorbing the excitation of 980 nm laser. The transition of $^2F_{7/2} \rightarrow {}^2F_{5/2}$ is usually resonant with the f–f transition of Er^{3+}, Ho^{3+} and Tm^{3+}, prompting the efficient energy transform from Yb^{3+} to these ions. For LNO:Yb^{3+}/Er^{3+}, the ground state $^4I_{15/2}$ of Er^{3+} is excited to the state $^4I_{11/2}$. Then under the effect of ET mechanism of Yb^{3+} → Er^{3+}, the excited electrons on the level $^4I_{11/2}$ are partly excited to the energy level $^4F_{7/2}$. Afterwards, the electrons relax from $^4F_{7/2}$ to $^2H_{11/2}$, $^4S_{3/2}$, generating green $^2H_{11/2}$, $^4S_{3/2} \rightarrow {}^4I_{15/2}$ transition. In another case, if the excited electrons on the energy level $^4I_{11/2}$ are relaxed to the energy level $^4I_{13/2}$ accompanied by another timely ET from Yb^{3+} to the energy level $^4I_{13/2}$ of Er^{3+}, the energy from $^4I_{13/2}$ will be transferred to $^4F_{9/2}$, and subsequently return to the ground state *via* radiative transition, producing red $^4F_{9/2} \rightarrow {}^4I_{15/2}$ transition.[32–35] For LNO:Yb^{3+}/Ho^{3+}, the mechanism is somewhat different from LNO:Yb^{3+}/Er^{3+}. The ground state absorption (GSA) is the phonon assisted process because the excitation energy between donor and acceptor could not match well (about 1580 cm^{-1}) and hence there is no resonant transition. Firstly, the energy of Ho^{3+} ions is excited from the ground state $^5I_8$ to the excited state $^5I_6$ *via* phonon-assisted ET. Following this process, the second photon absorbed from energy level $^2F_{5/2}$ of Yb^{3+} or the second pump photons make Ho^{3+} excite to the state $^5F_4$, $^5S_2$ and then decay to the ground state or the state $^5I_7$, in which process green $^5F_4$, $^5S_2 \rightarrow {}^5I_8$ and NIR $^5F_4$, $^5S_2 \rightarrow {}^5I_7$ are produced. If direct multiphotons relax to the energy level from $^5F_4$, $^5S_2$ to $^5F_5$, a strong red emission $^5F_5 \rightarrow {}^5I_8$ can be generated.[36,37] Non-radiative multiphoton relaxation rate also determines the efficiency of the UCL through impacting the population of the intermediate and the emitting levels. The non-radiative multiphoton relaxation rate constant is expressed as below:

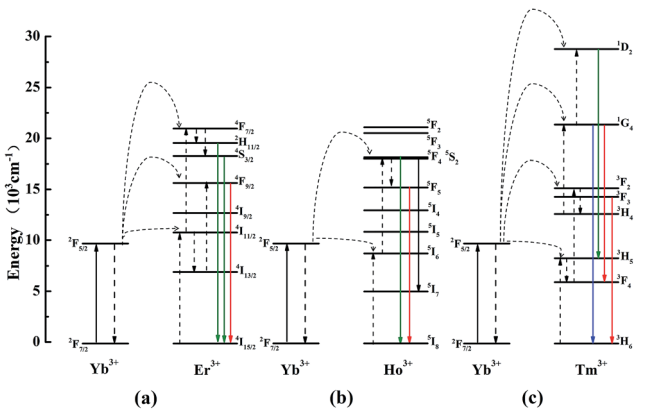

Fig. 7 The energy level diagrams of LNO:Yb^{3+}/Er^{3+}, LNO:Yb^{3+}/Ho^{3+}, LNO:Yb^{3+}/Tm^{3+} samples up-conversion mechanisms under 980 nm laser excitation.

$$k_{nr} \propto \exp(-\beta \Delta E / h\omega_{max})$$

where k_{nr} represents the multiphoton relaxation rate constant, β is the empirical constant, ΔE is the energy gap, and $h\omega_{max}$ is the highest energy vibrational mode of the host lattice. From the formula, k_{nr} decreases exponentially accompanied by the rise of energy gap. Compared with Yb^{3+} and Er^{3+}, Ho^{3+} is more likely to realize non-radiative multiphoton relaxation, which probably reducing the efficiency of Ho^{3+}.[38] For LNO:Yb^{3+}/Tm^{3+}, Tm^{3+} ions are excited from ground state $^3H_6$ level to $^1G_4$ level by three energy transfer processes and the mechanism is expressed as follows: firstly, $^3H_6$ (Tm) + $^2F_{5/2}$ (Yb) → $^3H_5$ (Tm) + $^2F_{7/2}$ (Yb), and then the energy level $^3H_5$ relaxes to $^3F_4$. Secondly, $^3F_4$ (Tm) + $^2F_{5/2}$ (Yb) → $^3F_2$ (Tm) + $^2F_{7/2}$ (Yb), and next go back to the energy level $^3H_4$ or $^3F_3$ by relaxation progress corresponding to the red emission $^3F_3$ → $^3H_6$. Lastly, $^3H_4$ (Tm) + $^2F_{5/2}$ (Yb) → $^1G_4$ (Tm) + $^2F_{7/2}$ (Yb). The photons transfer from the energy level $^1G_4$ to the ground state or $^3F_4$ level, corresponding to blue color $^1G_4$ → $^3H_6$ or red color $^1G_4$ → $^3F_4$. Another excited energy from Yb^{3+} excites the photons from $^1G_4$ to $^1D_2$ and decay to $^3H_5$ level resulting in relative weak green emission $^1D_2$ → $^3H_5$.[39–41]

The concentration of sensitizer and activator is a significant factor of the UCL properties. The concentration affects the relative amount of Ln^{3+} in the samples and the average distance between adjacent dopant ions, leading to a significant impact on the optical properties of the samples. Fig. 8 exhibit various UCL spectra under 980 nm excitation for LNO:*y*Yb^{3+},*e*Er^{3+}/*h*Ho^{3+}/*t*Tm^{3+} ($y = 0.02$–0.25, $e = 0.005$–0.04, $h = 0.0025$–0.02, $t = 0.001$–0.006) with different concentrations of up-conversion Ln^{3+} ions, respectively. All the as-prepared samples have the similar spectral profiles apart from the UCL intensity, indicating the crystal field is nearly consistent. Overall, as the concentration of Yb^{3+}, Er^{3+}/Ho^{3+}/Tm^{3+} ions increases, the emission intensities of them in the LNO:*y*Yb^{3+},*e*Er^{3+}/*h*Ho^{3+}/*t*Tm^{3+} systems are clearly rising to the maximum at $y = 0.1$, $e = 0.02$; $y = 0.15$, $h = 0.005$; $y = 0.15$, $t = 0.003$ and descending subsequently. The spectra of Er^{3+}, Ho^{3+} and Tm^{3+} with different concentration are shown in Fig. 8a–c. When the concentrations

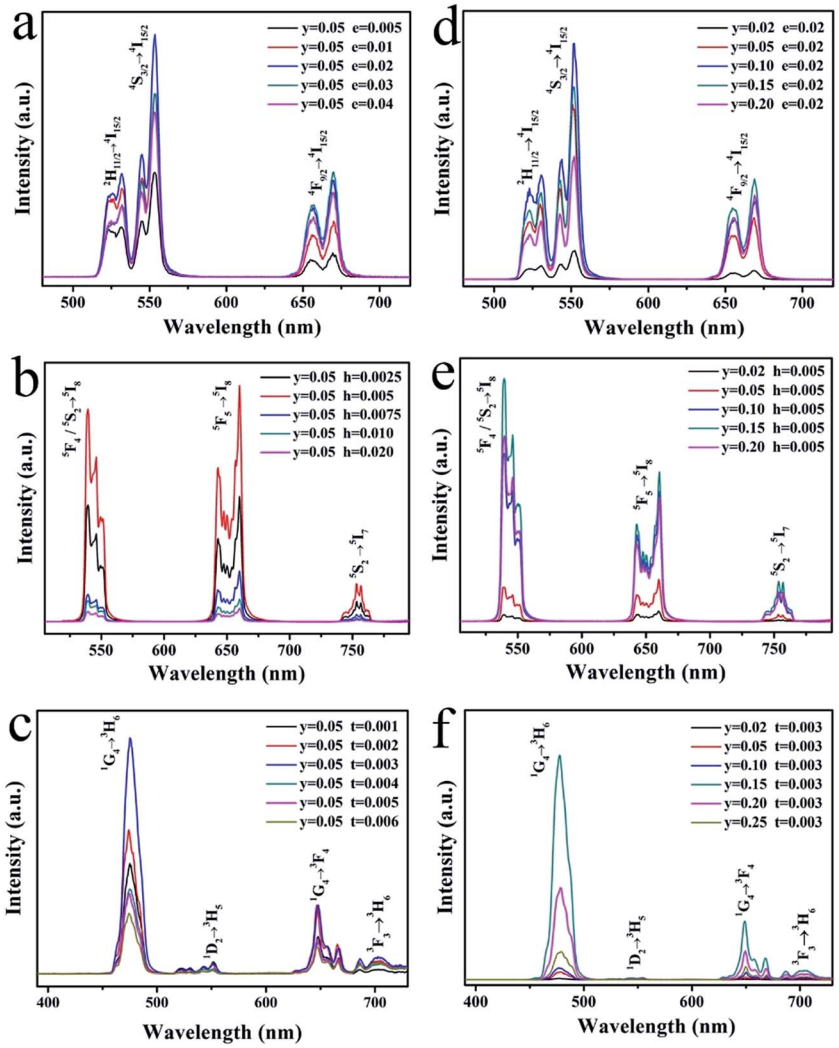

Fig. 8 Dependence of UCL emission spectra of (a) LNO:0.05Yb^{3+},*e*Er^{3+}, (b) LNO:0.05Yb^{3+},*h*Ho^{3+}, (c) LNO:0.05Yb^{3+},*t*Tm^{3+}, (d) LNO:*y*Yb^{3+},0.02Er^{3+}, (e) LNO:*y*Yb^{3+},0.005Ho^{3+}, (f) LNO:*y*Yb^{3+},0.003Tm^{3+}.

of Er^{3+}, Ho^{3+} and Tm^{3+} are lower than the maximum, the intensities of UCL keep rising corresponding to the increasing concentration. Energy transition is induced by the shorter distance between the activators, so the probability of energy transfers from sensitizer to activator increases.

Under the effect of cross-relaxation, the intensities decline occurs, when the concentrations surpass the optimal one. In Fig. 8d–f, as Yb^{3+} absorbing energy from 980 nm laser excitation, more and more energy can be absorbed and transferred to Ln^{3+} ions, leading to the enhancement of UCL intensities.[42] However, once the concentration of Yb^{3+} ions exceeds the maximum, concentration quenching occurs immediately. There are two explanations to account for the phenomenon: on the one hand, the pairing or aggregation of Yb^{3+} ions could induce a quenching effect. On the other hand, excessive Yb^{3+} ions act as the energy migrating bridge to defects, which can waste the excited energy through the non-radiative energy transition from Yb^{3+} ions to the defects.[43] The large absorption cross-section of Yb^{3+}, which minimizes the cross-relaxation energy loss, makes the activator content is relatively low(less than 2 mol%). In addition, from the spectra of Fig. 8a and d, the green emission of quenching concentration of LNO:yYb^{3+},eEr^{3+} is not equal to the red emission, which the maximum concentrations are respectively 0.1 and 0.15. The enhancement of Yb^{3+} concentration leads to a relative increase in the red emission intensity of Er^{3+}. A similar phenomenon has been found by other teams, and the factor on green emission and red emission has been studied. The reason for the variation of relative intensity of red ($^4F_{9/2} \rightarrow {}^4I_{15/2}$) and green emission ($^2H_{11/2}/{}^4S_{3/2} \rightarrow {}^4I_{15/2}$) is possibly the cross-relaxation process of $^2H_{11/2}/{}^4S_{3/2}$ (Er) + $^2F_{7/2}$ (Yb) $\rightarrow$ $^4I_{13/2}$ (Er) + $^2F_{5/2}$ (Yb), resulting in the population increasing on the $^4F_{9/2}$ level. Compared with $^4F_{9/2} \rightarrow {}^4I_{15/2}$ transitions, the $^2H_{11/2}/{}^4S_{3/2} \rightarrow {}^4I_{15/2}$ are restrained by the cross-relaxation process. In consequence, the phenomenon can be attributed to back-energy transition from Er^{3+} to Yb^{3+}.[44–46]

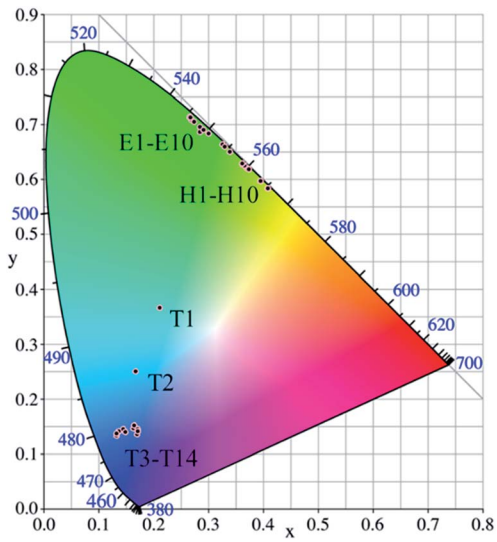

Fig. 9 CIE chromaticity diagram for LNO:yYb^{3+},eEr^{3+}(E1–E10), LNO:yYb^{3+},hHo^{3+}(H1–H10), LNO:yYb^{3+},tTm^{3+}(T1–T14) (y = 0.02–0.25, e = 0.005–0.04, h = 0.0025–0.02, t = 0.001–0.006).

Table 1 Variations of CIE chromaticity coordinate for LNO:yYb^{3+},eEr^{3+}, LNO:yYb^{3+},hHo^{3+}, LNO:yYb^{3+},tTm^{3+} (y = 0.02–0.25, e = 0.005–0.04, h = 0.0025–0.02, t = 0.001–0.006)

No. of points	LNO:yYb^{3+},0.02Er^{3+}		CIE(x, y)
E1	y = 0.02	e = 0.02	(0.26514, 0.71330)
E2	y = 0.05	e = 0.02	(0.26473, 0.71428)
E3	y = 0.10	e = 0.02	(0.26790, 0.71130)
E4	y = 0.15	e = 0.02	(0.26973, 0.70855)
E5	y = 0.20	e = 0.02	(0.28336, 0.69640)
No. of points	LNO:0.05Yb^{3+},eEr^{3+}		CIE(x, y)
E6	y = 0.05	e = 0.005	(0.26614, 0.71319)
E7	y = 0.05	e = 0.01	(0.27386, 0.70567)
E8	y = 0.05	e = 0.02	(0.28428, 0.68682)
E9	y = 0.05	e = 0.03	(0.29076, 0.69105)
E10	y = 0.05	e = 0.04	(0.29964, 0.68363)
No. of points	LNO:yYb^{3+},0.05Ho^{3+}		CIE(x, y)
H1	y = 0.02	h = 0.05	(0.39424, 0.59712)
H2	y = 0.05	h = 0.05	(0.37109, 0.61964)
H3	y = 0.10	h = 0.05	(0.33925, 0.65076)
H4	y = 0.15	h = 0.05	(0.32549, 0.66416)
H5	y = 0.20	h = 0.05	(0.32951, 0.66023)
No. of points	LNO:0.05Yb^{3+},hHo^{3+}		CIE(x, y)
H6	y = 0.05	h = 0.0025	(0.36330, 0.62725)
H7	y = 0.05	h = 0.005	(0.36480, 0.62580)
H8	y = 0.05	h = 0.0075	(0.40780, 0.58411)
H9	y = 0.05	h = 0.01	(0.36171, 0.62881)
H10	y = 0.05	h = 0.02	(0.37292, 0.61810)
No. of points	LNO:yYb^{3+},0.003Tm^{3+}		CIE(x, y)
T1	y = 0.02	t = 0.003	(0.21049, 0.36642)
T2	y = 0.05	t = 0.003	(0.16614, 0.25068)
T3	y = 0.10	t = 0.003	(0.16215, 0.14648)
T4	y = 0.15	t = 0.003	(0.13167, 0.13330)
T5	y = 0.20	t = 0.003	(0.13410, 0.13978)
T6	y = 0.25	t = 0.003	(0.14384, 0.14477)
T7	y = 0.30	t = 0.003	(0.13575, 0.14112)
T8	y = 0.35	t = 0.003	(0.13235, 0.13685)
No. of points	LNO:0.05Yb^{3+},tTm^{3+}		CIE(x, y)
T9	y = 0.05	t = 0.001	(0.15857, 0.16977)
T10	y = 0.05	t = 0.002	(0.17098, 0.14516)
T11	y = 0.05	t = 0.003	(0.14840, 0.13937)
T12	y = 0.05	t = 0.004	(0.16342, 0.15238)
T13	y = 0.05	t = 0.005	(0.16899, 0.13647)
T14	y = 0.05	t = 0.006	(0.17106, 0.14151)

The corresponding CIE coordinates positions as well as the chromaticity coordinates for the as-prepared LNO:yYb^{3+},eEr^{3+}/hHo^{3+}/tTm^{3+} samples under 980 nm laser excitation are shown in Fig. 9 and Table 1, respectively. It can be found that the emitted light of LNO:yYb^{3+},Er^{3+} samples shift from shorter wavelength to longer wavelength accompanied with increasing value of y, which exactly demonstrates the back-energy transition from Er^{3+} to Yb^{3+}. In addition, the chromaticity coordinates generally move regularly. When the ratio of Yb^{3+}/Ho^{3+} increases,

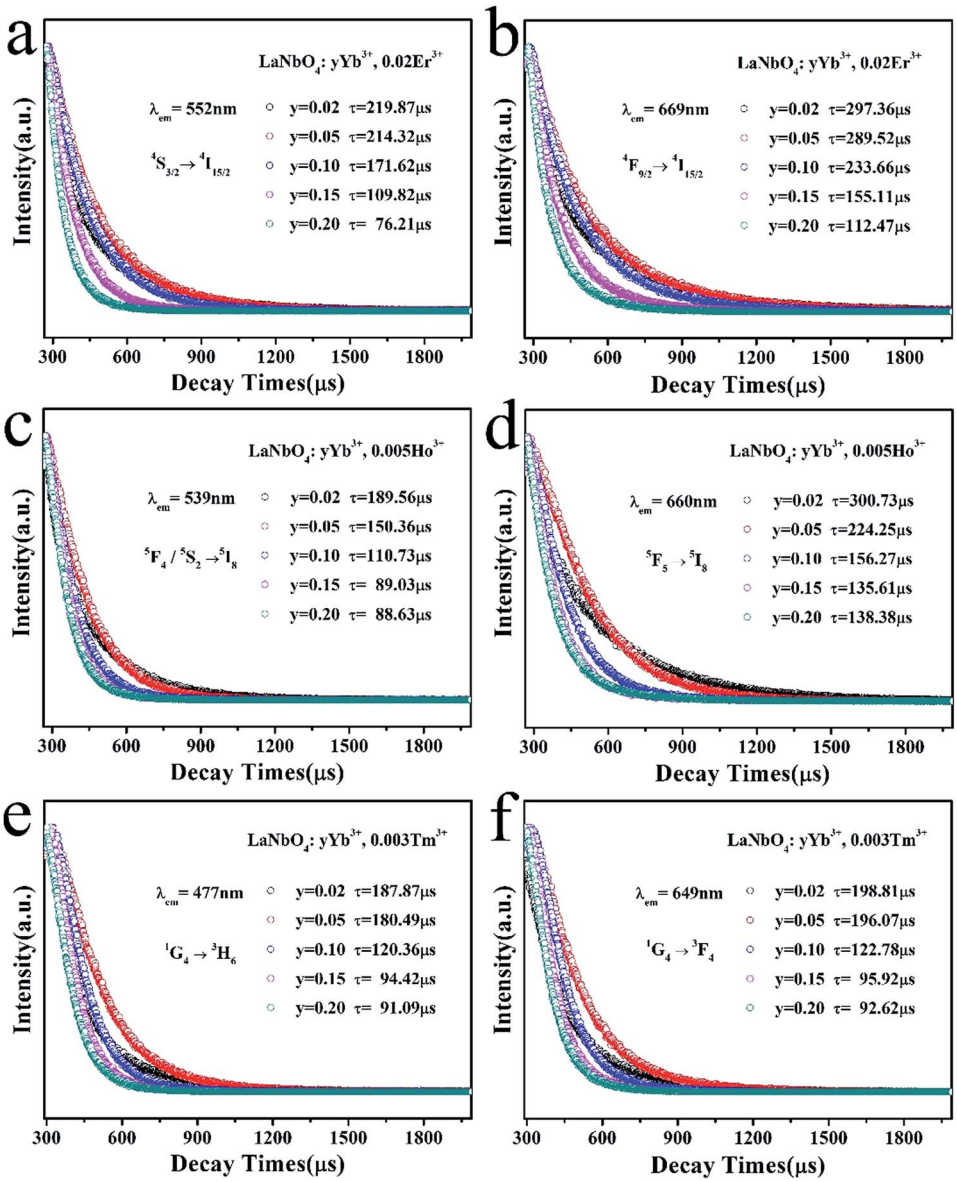

Fig. 10 Dependence of UCL decay lifetimes of (a and b) LNO:yYb^{3+},0.02Er^{3+} monitored at 552 nm and 669 nm, (c and d) LNO:yYb^{3+},0.005Ho^{3+} monitored at 539 nm and 660 nm, (e and f) LNO:yYb^{3+},0.003Tm^{3+} monitored at 477 nm and 649 nm, respectively.

the CIE positions shift from light yellow to green. It may be caused by the concentration of Yb^{3+}. For LNO:yYb^{3+}/tTm^{3+}, T1(LNO:0.02Yb^{3+},0.003Tm^{3+}), T2(LNO:0.05Yb^{3+},0.003Tm^{3+}) are respectively situated at (0.21049, 0.36642), (0.16614, 0.25068) corresponding to cyan and light blue and T3–T14 are assembled around dark blue area. Thus we can achieve different color through controlling the relative concentrations of sensitizer and activators.

To elucidate the quenching effect, we studied lifetimes of LNO:yYb^{3+},0.02Er^{3+} (monitored at 552 nm and 669 nm for $^4S_{3/2} \rightarrow {}^4I_{15/2}$ and $^4F_{9/2} \rightarrow {}^4I_{15/2}$), LNO:$y$Yb^{3+},0.005Ho^{3+} (monitored at 539 nm and 660 nm for $^5F_4/{}^5S_2 \rightarrow {}^5I_8$ and $^5F_5 \rightarrow {}^5I_8$) and LNO:$y$Yb^{3+},0.003Tm^{3+} (monitored at 477 nm and 649 nm for $^1G_4 \rightarrow {}^3H_6$ and $^1G_4 \rightarrow {}^3F_4$) under the excitation of a 980 nm laser as shown in Fig. 10. The decay curves of characteristic emissions are obviously changed with the concentration variation of Yb^{3+}. Generally, double-exponential decay behavior of the activators is usually accompanied with the energy transition from sensitizer to activator. Thus all of the samples can be well fitted with the double-exponential formula as follows:

$$I(\tau) = I_1 \exp(-t/\tau_1) + I_2 \exp(-t/\tau_2)$$

in the formula, I represents the fluorescent intensity, I_1, τ_1 and I_2, τ_2 are the shorter and longer lifetime constants, and t is the time. On the basis of above parameters, decay time can be calculated by the formula $\tau = (I_1\tau_1^2 + I_2\tau_2^2)/(I_1\tau_1 + I_2\tau_2)$, the values of calculated lifetimes were concluded and exhibited in Fig. 10. In general, we can observe that the value of τ decreases monotonously along with the increasing concentration of Yb^{3+} ion.

4. Conclusions

In summary, a series of Ln^{3+} (Yb^{3+}, Er^{3+}/Ho^{3+}/Tm^{3+}) ions doped LNO materials have been successfully prepared through a facile sol–gel process and subsequent combustion, and the up-conversion results are presented. The results of TG-DTA, XRD and SEM analyses demonstrate that the samples annealed at 1000 °C present as the monoclinic phase of LNO with no additional phases and exhibit homogeneous and spherical grains. Under 980 nm laser excitation, LNO:Yb^{3+}/Er^{3+}, LNO:Yb^{3+}/Ho^{3+}, LNO:Yb^{3+}/Tm^{3+} samples exhibit intense up-conversion emissions. The power-dependent UCL spectra of LNO:Yb^{3+},Er^{3+}/Ho^{3+}/Tm^{3+} indicate a two-photon absorption is the main process. The corresponding mechanism, including the emission, energy transfer, multi-phonon relaxation process, has been discussed detailedly. UCL multicolor fine-tuning can be achieved *via* changing the concentration of the dopant ions. We also receive the optimal UCL intensity, which are separately LNO:0.10Yb^{3+}/0.02Er^{3+}, LNO:0.15Yb^{3+}/0.005Ho^{3+}, LNO:0.15Yb^{3+}/0.003Tm^{3+}, respectively.

The relative variation of red and green emission for LNO:*y*Yb^{3+}/*e*Er^{3+} has also given detailed explanation. And meanwhile, spectra, emitting colors as well as lifetimes have been certified the relation with the concentration of Yb^{3+} ion. All in all, it can be concluded that we have found an excellent matrix to achieve efficient UCL emission. The UCL properties have shown potential application in the field of 3D display and solid-state lasers and provided a new insight to design a novel UCL materials with high efficiency.

Acknowledgements

The authors would like to acknowledge the financial support from National Science Foundation of Shandong Province (ZR2016EMM20, ZR2016EMQ09), the Science and Technology Foundation of Shenzhen, Shenzhen Science and Technology Innovation Committee (JCYJ20160331173823401) and National Science Foundation of China (51372138).

Notes and references

1 M. Haase and H. Schäfer, *Angew. Chem., Int. Ed.*, 2011, **50**, 5808.
2 X. Teng, Y. Zhu, W. Wei, S. Wang, J. Huang, R. Naccache, W. Hu, A. Y. Tok, Y. Han, Q. Zhang, Q. Fan, W. Huang, J. A. Capobianco and L. Huang, *J. Am. Chem. Soc.*, 2012, **134**, 8340.
3 M. Challenor, P. Gong, D. Lorenser, M. Fitzgerald, S. Dunlop, D. D. Sampson and K. S. Iyer, *ACS Appl. Mater. Interfaces*, 2013, **5**, 7875.
4 Q. C. Sun, H. Mundoor, J. C. Ribot, V. Singh, I. I. Smalyukh and P. Nagpal, *Nano Lett.*, 2013, **14**, 101.
5 J. H. Kim and J. H. Kim, *ACS Photonics*, 2015, **2**, 633.
6 S. Guo, X. Xie, L. Huang and W. Huang, *ACS Appl. Mater. Interfaces*, 2015, **8**, 847.
7 K. Yamamoto, M. Fujii, S. Sowa, K. Imakita and K. Aoki, *J. Phys. Chem. C*, 2015, **119**, 1175.
8 X. Chen, W. Xu, H. Song, C. Chen, H. Xia, Y. Zhu, D. Zhou, S. Cui, Q. Dai and J. Zhang, *ACS Appl. Mater. Interfaces*, 2016, **8**, 9071.
9 T. Liu, X. Bai, C. Miao, Q. Dai, W. Xu, Y. Yu, Q. Chen and H. Song, *J. Phys. Chem. C*, 2014, **118**, 3258.
10 A. Stepuk, G. Casola, C. M. Schumacher, K. W. Krämer and W. J. Stark, *Chem. Mater.*, 2014, **26**, 2015.
11 X. Ma and X. Ni, *J. Nanopart. Res.*, 2013, **15**, 1.
12 J. Yu, Y. Yang, R. Fan, D. Liu, L. Wei, S. Chen, L. Li, B. Yang and W. Cao, *Inorg. Chem.*, 2014, **53**, 8045.
13 J. Jin, Y. J. Gu, C. W. Y. Man, J. Cheng, Z. Xu, Y. Zhang, H. Wang, V. H. Y. Lee, S. H. Cheng and W. T. Wong, *ACS Nano*, 2011, **5**, 7838.
14 R. Wei, Z. Wei, L. Sun, J. Z. Zhang, J. Liu, X. Ge and L. Shi, *ACS Appl. Mater. Interfaces*, 2015, **8**, 400.
15 V. Muhr, S. Wilhelm, T. Hirsch and O. S. Wolfbeis, *Acc. Chem. Res.*, 2014, **47**, 3481.
16 X. Yu, M. Li, M. Xie, L. Chen, Y. Li and Q. Wang, *Nano Res.*, 2010, **3**, 51.
17 S. M. Ametamey, M. Honer and P. A. Schubiger, *Chem. Rev.*, 2008, **108**, 1501.
18 T. V. Esipova, X. Ye, J. E. Collins, S. Sakadžić, E. T. Mandeville, C. B. Murray and S. A. Vinogradov, *Proc. Natl. Acad. Sci. U. S. A.*, 2012, **109**, 20826.
19 D. Patel, A. Kell, B. Simard, B. Xiang, H. Y. Lin and G. Tian, *Biomaterials*, 2011, **32**, 1167.
20 X. Ge, L. Dong, L. Sun, Z. Song, R. Wei, L. Shi and H. Chen, *Nanoscale*, 2015, **7**, 7206.
21 F. Auzel, *Chem. Rev.*, 2004, **104**, 139.
22 Y. Lu, X. Tang, L. Yan, K. Li and X. Liu, *J. Phys. Chem. C*, 2013, **117**, 21972.
23 K. Li, Y. Zhang, X. Li, M. Shang, H. Lian and J. Lin, *Phys. Chem. Chem. Phys.*, 2015, **17**, 4283.
24 K. Li, X. Liu, Y. Zhang, X. Li, H. Lian and J. Lin, *Inorg. Chem.*, 2014, **54**, 323.
25 O. Ehlert, R. Thomann, M. Darbandi and T. Nann, *ACS Nano*, 2008, **2**, 120.
26 G. Blasse and L. H. Brixner, *Chem. Phys. Lett.*, 1990, **173**, 409.
27 F. Auzel, *Chem. Rev.*, 2004, **104**, 139.
28 J. Zhao, Y. Sun, X. Kong, L. Tian, Y. Wang, L. Tu, J. Zhao and H. Zhang, *J. Phys. Chem. B*, 2008, **112**, 15666.
29 F. Vetrone, V. Mahalingam and J. A. Capobianco, *Chem. Mater.*, 2009, **21**, 1847.
30 R. Balakrishnaiah, D. W. Kim, S. S. Yi, K. Jang, H. S. Lee and J. H. Jeong, *Opt. Mater.*, 2009, **31**, 959.
31 F. Wang and X. Liu, *Chem. Soc. Rev.*, 2009, **38**, 976.
32 J. Tang, L. Chen, J. Li, Z. Wang, J. Zhang, L. Zhang, Y. Luo and X. Wang, *Nanoscale*, 2015, **7**, 14752.
33 Y. Tian, Y. Tian, P. Huang, L. Wang, Q. Shi and C. Cui, *Chem. Eng. J.*, 2016, **297**, 26.
34 F. Zhang, G. Li, W. Zhang and Y. L. Yan, *Inorg. Chem.*, 2015, **54**, 7325.
35 W. Yao, Q. Tian, J. Liu, Z. Wu, S. Cui, J. Ding, Z. Dai and W. Wu, *J. Mater. Chem. C*, 2016, **4**, 6327.
36 P. Anurag, K. Vinod, R. E. Kroon and H. C. Swart, *J. Alloys Compd.*, 2016, **672**, 190.

37 A. Dwivedi, A. K. Singh and S. B. Rai, *Dalton Trans.*, 2014, **43**, 15906.
38 J. M. F. Van Dijk and M. F. H. Schuurmans, *J. Chem. Phys.*, 1983, **78**, 5317.
39 M. Rathaiah, P. Haritha, A. D. Lozano-Gorrín, P. Babu, C. K. Jayasankar, U. R. Rodríguez-Mendoza, V. Lavín and V. Venkatramu, *Phys. Chem. Chem. Phys.*, 2016, **18**, 14720.
40 H. Guo, N. Dong, M. Yin, W. Zhang, L. Lou and S. Xia, *J. Phys. Chem. B*, 2004, **108**, 19205.
41 M. Li, X. Liu, L. Liu, B. Ma, B. Li, X. Zhao, W. Tong and X. Wang, *Inorg. Chem.*, 2016, **3**, 1082.
42 D. Xu, C. Liu, J. Yan, S. Yang and Y. Zhang, *J. Phys. Chem. C*, 2015, **119**, 6852.
43 J. Wang, R. Deng, M. A. MacDonald, B. Chen, J. Yuan, F. Wang, D. Chi, T. S. A. Hor, P. Zhang, G. Liu, Y. Han and X. Liu, *Nat. Mater.*, 2014, **13**, 157.
44 G. Chen, G. Somesfalean, Y. Liu, Z. Zhang, Q. Sun and F. Wang, *Phys. Rev. B: Condens. Matter Mater. Phys.*, 2007, **75**, 195204.
45 D. Xu, C. Liu, J. Yan, S. Yang and Y. Zhang, *J. Phys. Chem. C*, 2015, **119**, 6852.
46 A. Li, D. Xu, Y. Zhang, H. Lin, S. Yang, Z. Chen and Y. Shao, *J. Am. Ceram. Soc.*, 2016, **99**, 1657.

